Prediction of Longitudinal Combustion Instability in a Solid-Propellant Rocket Motor

Jae-Kun Yoon*

(*Received December 1, 1993*)

The main objective of this technical paper is to demonstrate a capability which can predict the linear stability in a solid-propellant rocket motor using approximate stability analysis result which is based on spatial and temporal averaging of the equations for two-phase flow. The stability history of a rocket motor during burning can be showed along the time. To do this, a performance prediction of a rocket motor should be also carried out. The results derived from two sample calculations are presented and the limits of this analysis are discussed. This analysis is only for the longitudinal mode acoustic combustion instability in solid-propellant rocket motor.

Key Words: Combustion Instability, Acoustic Longitudinal Mode, Solid-Propellant Rocket Motor

Nomenclatures

A_b : Admittance function of the propellant
A_n : Admittance function of the nozzle
A_t : Nozzle throat area
$\bar{a}$: Speed of sound
a : Burning-rate constant
C : Specific heat of condensed material
C_D : Nozzle discharge coefficient
C_F : Thrust coefficient
C_M : Motor coefficient
C_m : Mass particle/mass gas
C_p : Specific heat of gas
E_n^2 : Defined in Eq. (8)
I : Stability integral
L : Grain length
$\bar{M}_b$: Mach number of flow at the propellant surface
$\bar{M}_n$: Mach number of flow at the nozzle entrance
M_w : Molecular weight of the propellant combustion products
m : Mass flux
n : Burning-rate exponent
P_a : Ambient pressure
P_c : Chamber pressure
P_e : Exit pressure
p : Pressure
R : Response function
R_u : Universal gas constant
S_b : Burning surface area
S_c : Cross-sectional area
S_n : Nozzle inlet area
T_c : Chamber temperature
t : Time
u : Velocity
α : Stability element
γ : Specific heat ratio
ψ_n : Mode shape function
μ : Viscosity
ρ_p : Propellant density
ρ_s : Particle density
σ : Particle diameter
κ_p : Thermal diffusivity of propellant
η_D : Discharge correction factor

Subscript

b : Burning surface
dc : Distributed combustion
ft : Flow turning
m : Motor

* Senior Researcher, Agency for Defense Development, Yuseong P. O. Box 35, Taejon, 305-600, Korea

n : Nozzle
p : Particle damping
pc : Pressure coupling
sd : Structural damping
vc : Velocity coupling

Superscript

$'$: Fluctuating component
$\tilde{}$: Complex component
(r) : Real component
$\bar{}$: Mean value

1. Introduction

For more than half a century, considerable time and money has been devoted to improve our understanding of combustion instability in solid rocket propulsion system. During this period, significant knowledge toward the prediction of the acoustic stability of solid propulsive systems has been accumulated.

If the system is stable, any random pressure perturbations that occur will dampen out. Conversely, if the system is dynamically disastrous consequences, from exceeding the guidance and control limits of the vehicle to destroying the propulsive system. In the development of any solid-propellant rocket motor, the dynamic combustion stability of the motor design, including the choice of propellant formulation.

The term linear instability refers to oscillations which are purely sinusoidal in nature. The term non-linear instability refers to oscillations which contain many acoustic modes and are often characterized by steep-fronted non-sinusoidal waveforms(Levine, 1974). This type of instability is often the result of injecta or debris passing through the nozzle and pulsing the motor. Non-linear oscillations are often accompanied by DC pressure shifts and limiting amplitudes of the oscillations. Although non-linear instability is an important aspect of solid-propellant motor stability, the scope of this paper is restricted to only linear instability in solid-propellant rocket motors.

The main objective of this paper is to demonstrate a capability which can predict the linear stability in solid-propellant rocket motor. Without a performance analysis, carrying out only the stability analysis of a rocket motor is almost impossible. Therefore, the limits of the performance prediction code are critical to this analysis. Stability and performance analysis are briefly explained and two sample calculations are carried out. This analysis is only for the longitudinal mode acoustic combustion instability in solid-propellant rocket motor.

2. Linear Stability Analysis

A small pressure disturbance varying sinusoidally in time inside a rocket chamber can be described as the real part of

$$p' = \tilde{p} e^{iwt} e^{\alpha_m t} \tag{1}$$

If $\alpha_m > 0$, the amplitude of the oscillations increases with time and is therefore unstable. If $\alpha_m < 0$, the amplitude decreases with time and the oscillations are stable.

The exponetial coefficient has been shown to have the general form

$$\alpha_m = \alpha_{pc} + \alpha_{vc} + \alpha_{dc} + \alpha_n + \alpha_p + \alpha_{ft} + \alpha_{sd} \tag{2}$$

where $_{pc}$ is pressure coupling, $_{vc}$ velocity coupling, $_{dc}$ distributed combustion, $_{n}$ nozzle damping, $_{p}$ particle damping, $_{ft}$ flow turning, and $_{sd}$ structural damping(Nickerson, 1983).

Stability elements represent the various gain and loss mechanisms, and several elements are generally expressed as a response function multiplied by a stability integral. The elements included are :

(1) Pressure coupling

$$\alpha_{pc} = R_{pc} I_{pc} \tag{3}$$

where R_{pc} is response function and I_{pc} is stability integral,

$$R_{pc} = \frac{\tilde{m}_b / \bar{m}_b}{\tilde{p} / \bar{\gamma} \bar{p}} \tag{4}$$

where m_b is mass flux at the burning surface. R_{pc} represents the response characteristics of the propellant and can be measured by the T-burner method(Culick, 1974). Figure 1 shows a typical pressure coupling response function which is curve-fitted by AB model(Denison, 1961). This

response function is very important and crucial to the motor stability. Because the pressure coupling response of the propellant is the strongest driving mechanism to make a rocket motor unstable.

(2) Velocity coupling

$$\alpha_{vc}=R_{vc}I_{vc} \tag{5}$$

$$R_{vc}=\frac{\hat{m}_b/\bar{m}_b}{\hat{u}/\bar{u}} \tag{6}$$

where R_{vc} represents the erosive characteristics of the propellant and should also be measured.

(3) Distributed combustion

Distributed combustion term is caused by the interaction of the acoustic field with burning metal particles taking place away from the surface of the propellant. In general, this term is very small except in the case of highly metallized propellants.

(4) Nozzle damping

This is the largest damping mechanism of longitudinal instability. When the acoustic waves contact the nozzle throat section, some of the acoustic energy is transmitted and radiated out of the nozzle.

(5) Particle damping

The amount of particle damping is very dependent on the mass fraction of particles in the flow field and, especially, on particle size. Larger particles damp lower frequencies while smaller particles damp out higher frequencies.

(6) Flow interaction

Mean/acoustic flow interaction losses are losses associated with interactions between mean flow and the acoustic field. The contribution of flow interaction to damping is often large, but its value is determined only by analysis based on the one-dimensional approximation to unsteady motions. Neither computational nor experimental methods have yet established the accuracy of the value.

(7) Structural damping

This is due to the deformation of the motor case caused by acoustic pressure oscillations. This value is very small.

The linear stability approach assumes that each of the acoustic energy gains and losses that contribute to motor stability can be individually computed from knowedge of the internal geometry of the motor as well as knowledge of the propellant, including products of combustion. One difficulty that is impossible to avoid is that each element in a collection of separate analyses of varying complexity cannot be expected to be of uniform quality. Since it is a system analysis that we need, the final analytical tool may be only as good as its weakest component.

Most contemporary predictions of linear stability(Nickerson, 1983; Culick, 1992) are based on the approximate analysis formulated by F.E.C. Culick(Culick, 1973). It is based on spatial and temporal averaging of the equations for two-phase flow. Detailed derivations are not necessary here: only final contributions(Culick, 1992) for a longitudinal combustion instability are listed.

$$\begin{aligned}\alpha_c&=\frac{\bar{a}}{2E_n^2}\iint(A_b^{(r)}+\bar{M}_b)\psi_n^2 dS_b\\&=\frac{\bar{a}}{2}(A_b^{(r)}+\bar{M}_b)\left[\frac{\int\int\psi_n^2 dS_b}{\int_0^L\psi_n^2 S_c dz}\right]\\&\approx\frac{\bar{a}}{2}\bar{M}_b\cdot R_b^{(r)}\left[\frac{\int\int\psi_n^2 dS_b}{\int_0^L\psi_n^2 S_c dz}\right]\end{aligned} \tag{7}$$

where

$$E_n^2=\int_0^L\psi_n\bar{\rho}'S_c dz\approx\int_0^L\psi_n^2 S_c dz \tag{8}$$

S_b is burning surface, assuming that $(A_b^{(r)}+\bar{M}_b)$ is constant over the burning surface.

$$\begin{aligned}\alpha_n&=-\frac{\bar{a}}{2E_n^2}\iint(A_n^{(r)}+\bar{M}_n)\psi_n^2 dS_n\\&=-\frac{\bar{a}}{2}(A_n^{(r)}+\bar{M}_n)\left[\frac{\int\int\psi_n^2 dS_n}{\int_0^L\psi_n^2 S_c dz}\right]\end{aligned}$$

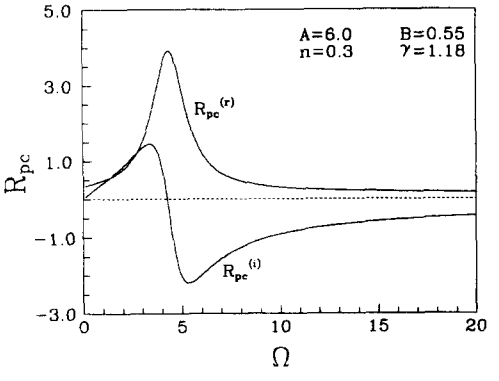

Fig. 1 Pressure coupling response function of a typical solid-propellant

$$\approx -\frac{\bar{a}}{2}\left(\frac{\bar{\gamma}+1}{2}\right)\bar{M}_n\left[\frac{\int\int \psi_n^2 dS_n}{\int_0^L \psi_n^2 S_c dz}\right] \quad (9)$$

where S_n is the nozzle inlet area. For longitudinal oscillations in a chamber of constant cross section, $\psi_n=\cos k_n z=\cos(\pi n z/L)$. Therefore,

$$\alpha_p=-\frac{1}{2}\frac{C_m}{1+C_m}\left[X_1\frac{1}{E_n^2}\iiint\left(\frac{\nabla\psi_n}{k_n}\right)^2 dV+(\bar{\gamma}-1)\frac{C}{\bar{C}_p}X_2\right]$$

$$=-\frac{1}{2}\frac{C_m}{1+C_m}\left[X_1+(\bar{\gamma}-1)\frac{C}{\bar{C}_p}X_2\right] \quad (10)$$

where

$$X_1=\frac{\omega_n\Omega_d}{1+\Omega_d^2}$$

$$X_2=\frac{\omega_n\Omega_t}{1+\Omega_t^2}$$

$$\Omega_d=\omega_n\tau_d$$

$$\Omega_t=\omega_n\tau_t$$

$$\tau_d=\frac{\rho_s\sigma^2}{18\mu}$$

$$\tau_t=\left(\frac{3}{2}\frac{C\mu}{\kappa_p}\right)\tau_d$$

Eqs. (7), (9) and (10), are used to calculate the stability elements. There is still room for extension to account for other contributions such as velocity coupling, distributed combustion and inert surface damping.

3. Performance Prediction Method

The burning rate of a propellant usually shows a strong pressure dependence that may be described by the empirical equation

$$r=aP_c^n \quad (11)$$

where a is an empirical constant influenced by the intial temperature of the propellant, and n is the burning rate pressure exponent. Without erosive burning and dynamic burning, the propellant can be assumed to burn normally across the entire surface. Under steady operating conditions, the mass burning rate of the propellant is

$$\dot{m}=\rho_p S_b r \quad (12)$$

where ρ_p is the propellant density, and S_b is the burning surface area. For a rocket motor, the mass flow rate produced by combustion of the solid propellant is equal to that of the exhaust gas. The gas mass flow rate through a choked nozzle can be written as

$$\dot{m}_g=C_D A_t P_c \quad (13)$$

where C_D, the nozzle discharge coefficient, can be expressed in terms of the molecular weight of the propellant combustion products M_w and the chamber temperature.

$$C_D=\frac{1}{C^*}=\sqrt{\gamma\left(\frac{2}{\gamma+1}\right)^{\frac{\gamma+1}{\gamma-1}}\frac{M_w}{R_u T_c}} \quad (14)$$

where R_u is the universal gas constant. From Eqs. (12), (13) and (14), chamber pressure P_c can be expressed as

$$P_c=\left[\frac{\bar{a}\rho_p S_b}{C_D A_t}\right]^{\frac{1}{1-n}} \quad (15)$$

The instantaneous burning surface area variation can be acquired in terms of trigonometric functions from grain geometry. A_t is given or optimized with the constraint of maximum D_e. C_D is calculated from the propellant properties of the output of CEC(Chemical Equilibrium Code). Therefore C_D is the ideal value. In real prediction, C_D is used as a value multiplied by the discharge correction factor, η_D, which is given experimentally or empirically. The thrust for a rocket motor is

$$F=C_F A_t P_c \quad (16)$$

where the thrust coefficient, C_F, can be expressed in terms of chamber pressure and exit pressure.

$$C_F=\sqrt{\frac{2\gamma^2}{\gamma-1}\left(\frac{2}{\gamma-1}\right)^{\frac{\gamma+1}{\gamma-1}}\left[1-\left(\frac{P_e}{P_c}\right)^{\frac{\gamma-1}{\gamma}}\right]}+\left[\frac{P_e-P_a}{P_c}\right]\frac{A_e}{A_t} \quad (17)$$

where P_a is ambient pressure. The pressure ratio $\frac{P_e}{P_c}$ can be acquired from the following equation.

$$\frac{A_t}{A_e}=\left(\frac{\gamma+1}{2}\right)^{\frac{1}{\gamma-1}}\left(\frac{P_e}{P_c}\right)^{\frac{1}{\gamma}}\sqrt{\frac{\gamma+1}{\gamma-1}\left[1-\left(\frac{P_e}{P_c}\right)\right]^{\frac{\gamma-1}{\gamma}}} \quad (18)$$

This is a one-dimensional, isentropic flow equation. In real prediction, C_F is used as a value multiplied by motor coefficient, C_M, which is given experimentally or empirically. A_b is changed as the burning proceeds, and A_t is increased if nozzle throat erosion occurs.

$$D_t = D_{to} - \dot{z} P_c^{0.8} t \tag{19}$$

where D_t, D_{to} and t represent throat diameter, initial throat diameter, burning time respectively. Nozzle throat erosion constant $\dot{z}$ can be determined experimentally.

4. Application and Discussion

Linear stability analysis is applied to two sample calculations to get the stability history versus time and additional perfromance prediction. The example cases are : (1) cylinder-type grain shape, and (2) star-type grain shape. When the grain is case-bonded and both ends of grain are inhibited, only internal burning occurs. Neither erosive burning nor dynamic burning can be accounted for.

4.1 Cylinder-shape grain

Figure 2 is a schematic diagram of a rocket motor. The numerical values of the quantities required in the input data file are listed below.

Geometrical properties :	
grain length	$L=596.9$ mm
diameter of cylindrical port	$D_c=50.6$ mm
throat diameter	$D_t=18.72$ mm
nozzle-exit diameter	$D_e=100$ mm
web thickness	$W_{eb}=10$ mm
Combustion properties :	
burning-rate constant	$a=0.04941$
burning-rate exponent	$n=0.3$
parameters in	$A=6.0$
combustion response	$B=0.55$
chamber temperature	$T=3539K$
mass particle/mass gas	$C_m=0.36$
particle diameter	$\sigma=2.0\times10^{-6}$ m
Physical properties :	
thermal diffusivity of propellant	$\kappa_p=1.0\times10^{-7}$ m^2/s
specific heat of gas	$C_p=2020$ J/kgK
specific heat of condensed material	$C=0.68C_p=1373.6$
viscosity	$\mu=8.925\times10^{-5}$ kg/ms
particle density	$\rho_s=4\times10^3$ kg/m^3
propellant density	$\rho_p=1{,}766$ kg/m^3
γ(gas only)	$\gamma=1.23$
$\bar{\gamma}$(mixture)	$\bar{\gamma}=\frac{[\gamma(1+C_mC/C_p)]}{(1+C_m\gamma C/C_p)}=1.18$
gas constant	$R=(\gamma-1)C_p/\gamma=377.72$ J/kgK
speed of sound in gas/particle mixture	$\bar{a}=\sqrt{(\bar{\gamma}RT_c)/(1+C_m)}=1075$ m/s
Mach number at the burning surface	$\bar{M}_b=\frac{\bar{u}_b}{\bar{a}}=\frac{(\rho_p/\rho)\bar{r}_b}{\sqrt{(\bar{\gamma}RT_c)/(1+C_m)}}=0.00173$

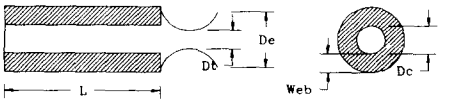

Fig. 2 Schematic diagram of rocket motor

Performance and stability elements curves versus time are Fig. 3. We can see that the cylinder-shape grain has progressive characteristics. Because cylinder grain has no sliver parts, predicted curve is terminated at the peak pressure and thrust. Instability-driving element is only α_c which decrease with time. This is due to the increase of cavity volume which is in the denominator of Eq. (7). Same reason can be adapted to decrease the aboslute value of α_n. Damping element α_p is constant with time. Because the sum of stability elements, α_t, is negative during the burn-

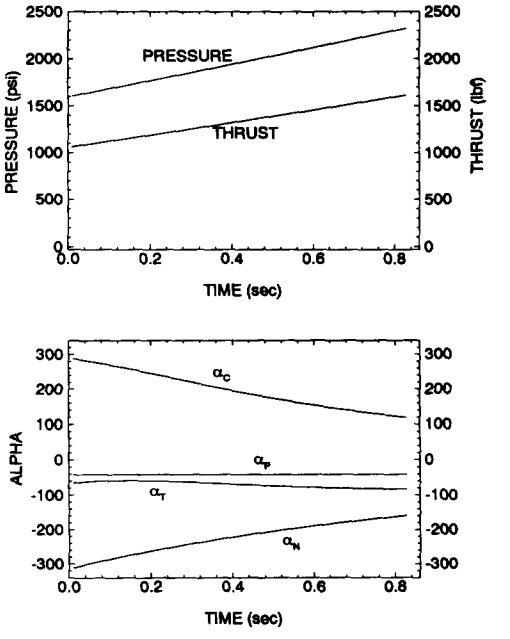

Fig. 3 Results of cylinder shape grain

ing, this motor can be considered stable. It should be noted that the minimum margin of stability occurs about 0.2 sec after ignition. The characteristic that stability margin has a minimum in the first half of the total burning time is typical in solid-propellant rocket motors.

4.2 Star-shape grain

Figure 4 is a schematic diagram of a 6-point star-shaped grain. The star shape is used broadly because of its neutral burning characteristics. Conversely, the cylinder-shape grain has progressive burning characteristics. With the star shape, a sliver of the propellant remains after the web is burned out, which causes tailing of the performance curve. The numerical values of the quantities required in the input data file are listed below.

Geometrical properties:

grain length	$L=150$ cm
diameter of grain	$D_F=12$ cm
inner radius of grain	$R_2=2$ cm
radius at grain top	$R_3=0.6$ cm
radius at star point	$R_4=0.3$ cm
angle of star sharpness	$\alpha_2=20$ degree
number of star points	$S_N=6$
web thikness	$Web=2$ cm

Combustion properties:

burning rate constant	$a=0.0397$
burning rate exponent	$n=0.444$
parameters in combustion response	$A=6.0$, $B=0.55$
chamber temperature	$T=3539$ K
mass particle/mass gas	$C_m=0.36$
particle diameter	$\sigma=2.0\times10^{-6}$ m

Physical properties:

thermal diffusivity of propellant	$\kappa_p=1.0\times10^{-7}$ m²/s
specific heat of gas	$C_p=2020$ J/kgK
specific heat of condensed material	$C=0.68C_p=1373.6$
viscosity	$\mu=8.925\times10^{-5}$ kg/ms
particle density	$\rho_s=4\times10^3$ kg/m³
propellant density	$\rho_p=1{,}728$ kg/m³
γ(gas only)	$\gamma=1.2559$
$\bar{\gamma}$(mixture)	$\bar{\gamma}=\dfrac{[\gamma(1+C_mC/C_p)]}{(1+C_m\gamma C/C_p)}=1.1957$
gas constant	$R=(\gamma-1)C_p/\gamma=411.52$ J/kgK
speed of sound in gas/particle mixutre	$\bar{a}=\sqrt{(\bar{\gamma}RT_c)/(1+C_m)}=1131.6$ m/s
Mach number at burning surface	$\bar{M}_b=\dfrac{\bar{u}_b}{\bar{a}}=\dfrac{(\rho_p/\rho)\bar{r}_b}{\sqrt{(\bar{\gamma}RT_c)/(1+C_m)}}=0.00173$

Performance curve and stability elements versus the time curve are shown in Fig. 5. The trends stability elements with time for the star-shaped grain are almost identical to those in the cylinder-shaped grain. However, α_c has a relatively large

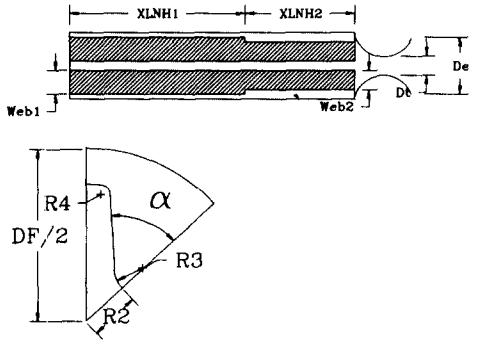

Fig. 4 Schematic diagram of star shape grain

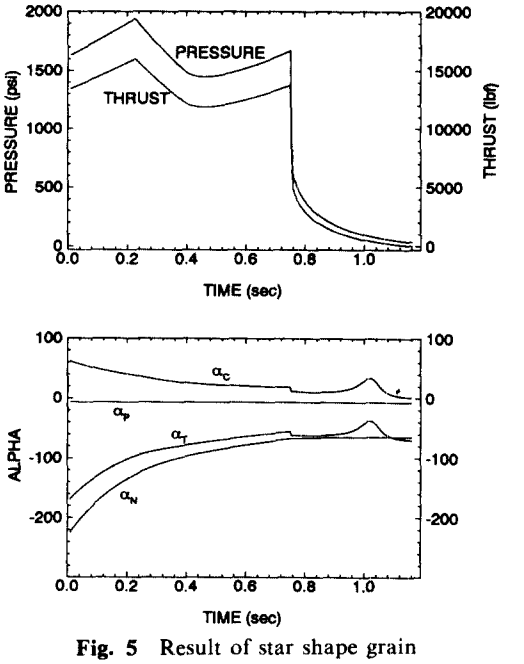

Fig. 5 Result of star shape grain

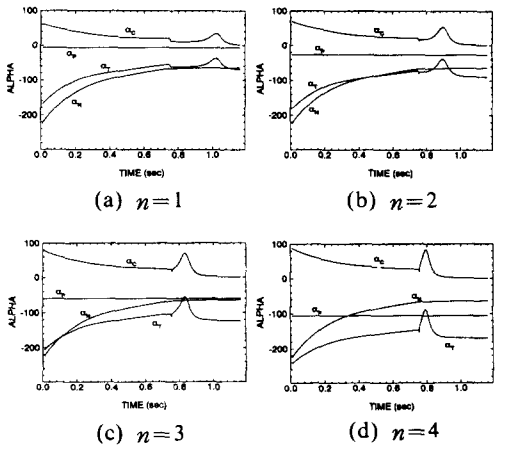

(a) $n=1$ (b) $n=2$

(c) $n=3$ (d) $n=4$

Fig. 6 Stability diagram for various longitudinal modes

peak around 1.0 sec due to matching of the peak of combustion response function $R_{pc}^{(r)}$. The stability margin therefore has a minimum of around 1.0 sec which does not appear to cause any stability problem. Because most of the burning has already ended and the mean pressure is very small. Figure 6 shows the results obtained by varying longitudinal mode shapes. The higher the longitudinal mode-shape number, and the sharper the peak of α_c, the sooner the peak will occur. For the fourth longitudinal-mode shape number, this peak coincides with the web-burnout time. Therefore, the high longitudinal mode instabiling around web-burnout time is of great concern. Fortunately, particle damping element α_p increases with mode-shape number. The predicted value shows that the margin of stability increase with mode-shape number.

5. Conclusions

Simply stated, a linear stability analysis or solid-propellant rocket motors with constant cross-section grain cavities is performed. This constraint of constant cross-section grain cavity is due to performance prediction methad. The linear stability analysis has no restrictions. So, if more general performance predition code is available, this stability analysis can be extended.

So far, there are no means to verify this analysis with experimental data. This is due to the lack of response function data of the propellant. Therefore, if reliable response function data are accumlated, this analysis will be tested for its reliability.

Acknowledgements

The author would like to express his deepest appreciation to Prof. Vigor Yang of The Pennsylvania State University for his guidance, support, and encouragement throughout the course of this work and to Dr. Y. K. Kim of ADD for providing his original performance prediction program.

References

Anon., 1971, *Solid Rocket Motor Performance Analysis and Prediction*, NASA-SP-8039.

Anon., 1972, *Solid Propellant Grain Design and Internal Ballistics*, NASA-SP-8076.

Culick, F. E. C., 1970, "Stability of Longitudinal Oscillations with Pressure and Velocity Coupling in a Solid Propellant Rocket Motor," Combustion Science and Technology, Vol. 2, pp. 179~201.

Culick, F. E. C., 1973, "The Stability of One-Dimensional Motions in a Rocket Motor," Combustion Science and Technology, Vol. 7, pp. 165~175.

Culick, F. E. C., 1974, "T-Burner Testing of Metallized Solid Propellants," Air Force Rocket Propulsion Laboratory, Rept. AFRPL-TR-74-28.

Culick, F. E. C. and Yang, V., 1992, "Prediction of the Stability of Unsteady Motions in Solid-Propellant Rocket Motors," *Nonsteady Burning and Combustion Stability of Solid Propellants*, edited by L. De Luca, E. W. Price and M. Summerfield, Vol. 143, Progress in Astronautics and Aeronautics, AIAA, Chap. 18.

Denison, M. R. and Baum, E., 1961, "A Simplified Model of Unstable Burning in Solid Propellants," American Rocket Society Journal, Vol. 31, No. 8, pp. 1112~1122.

Levine, J. N. and Culick, F. E. C., 1974, "Nonlinear Analysis of Solid Rocket Combustion Instability," Ultrasystems, Inc., AFRPL TR-74-

45.

Nickerson, G. R., Culick, F. E. C. and Dang, L. G., 1983, "Standard Stability Prediction Method for Solid Rocket Motors, Axial Mode Computer Program, User's Manual," Software and Engineering Associates, Inc., AFRPL TR-83-017.